



# OPEN Machine learning-enabled prediction of hemorrhagic transformation post-thrombectomy using quantitative DSA

Hui Li<sup>1,2</sup>, Chao Pang<sup>1,2</sup>, Xiaoying Guo<sup>1</sup>, Yufan Gui<sup>1</sup>, Xiangyu Meng<sup>1</sup>✉ & Conghui Li<sup>1</sup>✉

This study aims to construct a predictive model for post-thrombectomy hemorrhagic transformation (HT) by integrating hemodynamic features derived from quantitative DSA (qDSA) with machine learning models. A retrospective analysis was conducted on patients with acute anterior circulation large-vessel occlusion who underwent MT at our center from January to December 2024. Immediate postoperative anteroposterior and lateral angiograms of the target vessels were obtained after MT. Hemodynamic features such as mean transit time (MTT) and time to peak (TTP) were all calculated based on the time density curve derived from postoperative DSA. Clinical baseline data and interventional procedural information were also collected. Hemodynamic features associated with post-thrombectomy HT were selected using 5 different feature selection algorithms. Five machine learning models were employed to fit the features influencing the outcomes, and the results were evaluated using the Receiver operating characteristic (ROC) curves. The predictive performance of different models was compared using the area under the curve (AUC). SHapley Additive exPlanations (SHAP) were used for model interpretation. A total of 171 patients with anterior circulation large-vessel occlusion who underwent MT were included. Hemorrhagic transformation occurred in 68 patients. In contrast, the non-HT group comprised patients with the absence of intracranial hemorrhage or large cerebral infarction or cerebral herniation. In 171 patients, 39 hemodynamic parameters within the ROIs of the target vessels were extracted from perfusion images generated by postoperative DSA in each patient. After feature selection, the best-performing model on the testing set was the Elastic-Logistic model consisted of qDSA and clinical features, with an average AUC of 0.86. And the best-performing model on the testing set consisted of qDSA features alone, was the most frequently selected qDSA features still constructed using a logistic model, with an average AUC of 0.81. By integrating clinical and hemodynamic features, machine learning algorithms can be effectively utilized to construct a preliminary predictive model for post-thrombectomy HT in patients with acute ischemic stroke treated by mechanical thrombectomy.

**Keywords** Quantitative DSA, Hemodynamic features, Machine learning, Feature selection

Mechanical thrombectomy (MT) has become a well-established and highly effective treatment for acute ischemic stroke (AIS) caused by large vessel occlusion<sup>1,2</sup>. However, despite technically successful procedures, only 40%–50% of AIS patients get functional independence, highlighting the emergency need to identify factors contributing to poor clinical outcomes<sup>3–6</sup>. Among the most critical determinants of adverse outcomes is hemorrhagic transformation (HT), including cerebral hemorrhage and contrast extravasation, both of which significantly worsen prognosis and prolong hospitalization. Emerging evidence suggests that hyperperfusion plays a key role in HT following endovascular recanalization<sup>7</sup>. However, post-recanalization reperfusion assessment remains limited in clinical practice, primarily due to the difficulty of the process and radiation exposure associated with serial computed tomographic perfusion (CTP) scans<sup>8,9</sup>. While the Thrombolysis in

<sup>1</sup>Department of Neurosurgery, the first hospital of Hebei Medical University, Hebei Medical University, Shijiazhuang, China. <sup>2</sup>Hui Li and Chao Pang contributed equally to this work. ✉email: mengyu629@126.com; 13363880072@163.com

Cerebral Infarction (TICI) grading system provides a simply estimate of vascular reperfusion on angiography, it fails to capture microcirculatory perfusion status—a critical gap in current evaluation methods.

Quantitative digital subtraction angiography (qDSA) addresses this limitation by offering a semi-quantitative approach to hemodynamic assessment<sup>10</sup>. Through time-density curve analysis, qDSA derives key parameters such as time-to-peak (TTP), enabling comprehensive post-MT evaluation without requiring additional imaging procedures. Previous studies have established correlations between qDSA-derived metrics (e.g., mean transit time and TTP) and clinical outcomes in MT-treated AIS patients<sup>11</sup>. Notably, recent work introduced a novel composite perfusion index integrating ipsilateral and contralateral hemodynamic data, demonstrating significant prognostic value for guiding intraoperative decisions and postprocedural management<sup>12</sup>. Earlier investigations also revealed a U-shaped relationship between mean transit time and post-MT HT, though technological constraints at the time limited parameter extraction<sup>13</sup>.

While these findings highlight the potential of hemodynamic parameters for outcome prediction, important limitations persist. Current approaches often fail to account for complex interactions between multiple parameters and regional hemodynamic variations, potentially overlooking critical predictive factors. This knowledge gap hinders the development of personalized hemodynamic assessments that could optimize clinical decision-making.

To address these challenges, this study employs advanced machine learning algorithms to integrate multidimensional qDSA-derived hemodynamic parameters, constructing a robust predictive model for post-MT HT. By systematically quantifying relationships between perfusion characteristics and HT risk, our work aims to provide a data-driven foundation for early intervention strategies and personalized management in AIS patients following successful recanalization.

## Methods

### Study population

We conducted a retrospective analysis of consecutive AIS patients who underwent successful mechanical thrombectomy (MT) for anterior circulation large vessel occlusion at our single-center between January 2024 and December 2024. Patients were enrolled based on the following criteria: (1) age > 18 years; (2) Pre-stroke modified Rankin Scale (mRS) score  $\leq 2$ ; (3) Confirmed anterior circulation large vessel occlusion on diagnostic DSA meeting intervention criteria: Presenting within 6 h of symptom onset or presenting 6–24 h onset and meeting DAWN or DEFUSE-3 trial eligibility; (5) Successful recanalization post-MT (expanded Thrombolysis in Cerebral Infarction [eTICI] score  $\geq 2b$ ); (6) Availability of 6-hour postprocedural head CT for HT evaluation; Exclusion criteria were: (1) Severe pre-existing organ dysfunction (e.g., hepatic, renal, or cardiac failure); (2) Pre-existing hemorrhage identified in pre-treatment CT scan; (3) Posterior circulation or bilateral occlusions; (4) Incomplete or technically inadequate DSA series, poor image quality; (5) large-area cerebral infarct (the Alberta Stroke Program Early CT Score  $< 6$ ); (6) Postoperative CT showing either massive infarction with herniation (despite absence of HT) or indeterminate imaging findings. The reason for excluding these patients was that, though patients with large-area cerebral infarction or cerebral herniation had no hemorrhagic events, they still had abnormal hemodynamic status. Whereas the aim of this study was to establish a model capable of predicting simple hemorrhage or extravasation, with completely normal patients designated as negative labels. Thus, excluding such patients was intended to make the negative and positive labels more homogeneous. The primary outcome was radiologically confirmed hemorrhagic transformation (HT), defined as new hyperdense lesions on 6-hour post-MT non-contrast CT. Subarachnoid hemorrhage (SAH) cases were included with reperfusion-related and vessel ruptures due to manipulation were excluded. Patients were categorized as: Positive cases - demonstrated definite HT (parenchymal hematoma or hemorrhagic infarction); Negative cases - showed no HT or large cerebral infarction or cerebral herniation on post-operative CT scan. We excluded patients developing massive infarction with herniation (despite the absence of HT) as these represent a distinct pathophysiological entity with different hemodynamic profiles that would confound our predictive modeling. The institutional review board approved this retrospective study and waived the requirement for informed consent in accordance with local regulations and the study's observational nature.

### Clinical variable collection

The following data were collected for each patient: demographic features, medical history (including hypertension, atrial fibrillation, stroke or transient ischemic attack (TIA), and diabetes), and symptoms at the time of stroke onset. The severity of symptom onset was assessed using the National Institutes of Health Stroke Scale (NIHSS) and Glasgow Coma Scale (GCS). Laboratory test results at admission were also recorded. Additionally, relevant treatment-related indicators were obtained, including the administration of intravenous thrombolysis, onset-to-puncture time, puncture-to-recanalization time, location of target artery, number of thrombectomy attempts, mechanical thrombectomy (MT) techniques used, and eTICI scores following recanalization. Successful recanalization was defined as an eTICI score of 2b-3, and the collateral circulation was assessed by the American Society of Interventional and Therapeutic Neuroradiology/Society of Interventional Radiology (ASTIN/SIR) score. The mechanical thrombectomy techniques employed included thrombus aspiration, stent retriever thrombectomy, balloon dilation, and stent implantation. Dual antiplatelet therapy or tirofiban was administered only to patients who underwent stent implantation, consistent with our institutional protocol for stent-assisted thrombectomy. Patients without stenting received individualized antiplatelet therapy (e.g., single-agent aspirin or clopidogrel) based on clinical assessment.

### Quantitative digital subtraction angiography evaluation

In our study, all DSA images were acquired following a standardized protocol, utilizing a contrast injection method that was consistent across all patients. Following mechanical thrombectomy, both coronal and sagittal DSA

images were obtained of the target vessel to assess its patency. The angiographic procedure involved advancing the catheter into the internal carotid artery (ICA), followed by the injection of a contrast agent at a rate of 4 mL/s, with a total volume of 6 mL administered. Subsequently, systematic contrast acquisition was initiated with a 1-second delay after contrast injection, and DSA images were captured at a frequency of 4 frames per second. Five circular regions of interest (ROIs) were strategically positioned along the target vessels. These included the petrous segment (C2) of the internal carotid artery (designated as ROI1), the posterior communicating segment (C7) of the internal carotid artery (ROI2), the M1 segment (ROI3) and the M3 segment (ROI5) of the middle cerebral artery, as well as the A1 segment (ROI4) of the anterior cerebral artery. ROI1, located at the petrous segment of the internal carotid artery, served as the reference point to account for potential variations in hemodynamic characteristics due to catheter positioning and contrast agent concentration. Representative examples of the placement of each ROI are illustrated in Fig. 1. After the placement of the ROIs, a time-density curve (TDC) was generated from the data within these regions. The TDC was then fitted using a gamma variate function, which was implemented through a custom-developed program written in Python. The algorithms utilized for this process were created using the open-source Scipy Toolkit in Python. Hemodynamic parameters within each ROI were calculated based on the fitted TDC using the Gamma algorithm. These parameters included time to peak (TTP), mean transit time (MTT), full width at half maximum (FWHM), inflow gradient (wash-in slope, WIS), and outflow gradient (wash-out slope, WOS). Additionally, the following hemodynamic parameters were computed: stasis index (SI), relative value of TTP, MTT, and FWHM. The stasis index (SI) was defined as the ratio of the inflow gradient to the outflow gradient of the arterial ROI, which reflects the degree of blood flow patency. The delineation of the ROI was jointly performed by two experienced neuroradiologists with more than 5 years of interventional surgery. Both observers were blinded to patient outcomes, occlusion sites, and clinical data during ROI placement—reducing bias from prior knowledge. All inter-observer discrepancies ( $\leq 3\%$  of cases) were reviewed by a third senior neuroradiologist (with  $> 10$  years of experience) to reach consensus, ensuring consistency. The TDC-derived data (TTP, MTT, WIS and WOS) were subjected to Intraclass Correlation Coefficient (ICC) testing, where stable features with good consistency ( $ICC > 0.75$ ) were retained and averaged for subsequent analysis. The relative values were determined using the following method: With ROI1 serving as the reference, the relative value was defined as the difference between the qDSA values (TTP, MTT, and FWHM) of ROI3, ROI4, ROI5, and ROI1.

### Feature selection and machine learning model construction

Hemodynamic features (qDSA) were selected using five filter-based feature selection (FS) methods, including Relief, ElasticNet, DecisionTree, Lasso-regression, and Mutual-Information. The primary goal of these methods was to eliminate irrelevant features before ranking the remaining features. The top ten qDSA features with the highest feature coefficients were selected as the input features for machine learning model construction. For each feature selector, the selected features were assigned weights based on their ranking. The feature ranked first was assigned a weight of 1, while the feature ranked tenth was assigned a weight of 0.1, with intermediate rankings assigned weights accordingly. For example, in the Lasso selector, A1 TTP (relative), C7 FWHM, and A1 FWHM were assigned weights of 1, 0.5, and 0.1, respectively. After the features' weights ranking, the most selected qDSA features with the cumulative weights  $> 1.5$  were also applied to construct the machine learning models. Additionally, for the clinical features, univariate regression analysis was used to determine which features exhibited significant differences in predicting postoperative bleeding, with a significance threshold of  $p < 0.1$ . The selected clinical factors were combined with the qDSA hemodynamic features selected by the feature selection methods to construct a comprehensive clinical-hemodynamic model. We applied five supervised machine learning (ML) algorithms for classification: XGBoost classifier (initial learning rate: 0.0001, initial  $n_{\text{estimators}} = 100$ ), Adaboost classifier (initial learning rate: 0.01, initial  $n_{\text{estimators}} = 50$ ), random forest (RF, initial  $n_{\text{estimators}} = 100$ ), logistic regression (LG, solver = "liblinear"), and support vector machines (SVM, kernel = "linear", "rbf"). These classifiers were all imported from the Python (version 3.8) machine learning library named scikit-learn (version 20.0). Finally, a total of 30 qDSA models (25 models were constructed using 5 FS and 5 ML algorithms, 5 models were constructed using the most frequently selected qDSA features and 5 ML algorithms) were constructed using the hemodynamic features. In addition to the models described earlier, another 30 models were constructed using integrating the clinical features.

Each of the models was trained using the training dataset, with stratified data splitting implemented via the StratifiedShuffleSplit function from the scikit-learn library. This method ensures that each subset contains approximately the same percentage of samples of each target class as the original dataset. The entire dataset was divided into training and testing datasets at a ratio of 9:1 based on a per-patient basis. Specifically, the training set consisted of 153 patients, with 61 cases labeled as HT, accounting for 39.9% (61/153). The testing set included 18 patients, among whom 7 cases were HT, representing a proportion of 38.9% (7/18). Notably, the label ratios of both sets were basically consistent with that of the original dataset. During model training, a 5-fold cross-validation and the grid search approach was employed to optimize and determine the hyperparameters. To enhance the scientific validity and credibility of the results, five random seeds were used to perform five rounds of splitting on the entire dataset during the division of training and test sets. Subsequently, model training was conducted separately under each combination of the split datasets. The predictive performance of each classifier was assessed using the area under the receiver operating characteristic curve (AUC) and accuracy (ACC). After training, the models were tested on the independent test dataset, and their classification performance was also evaluated using AUC and ACC. Subsequently, the calculated AUC and ACC were used to compute the average AUC and ACC across datasets with different random seeds, so as to enhance the credibility of the results. The feature selection (FS) and machine learning processes were implemented using Python (version 3.8). For the statistical analysis of clinical, continuous variables were presented as medians with interquartile ranges (IQR). The differences between groups were compared using the Mann-Whitney U test. For categorical variables,

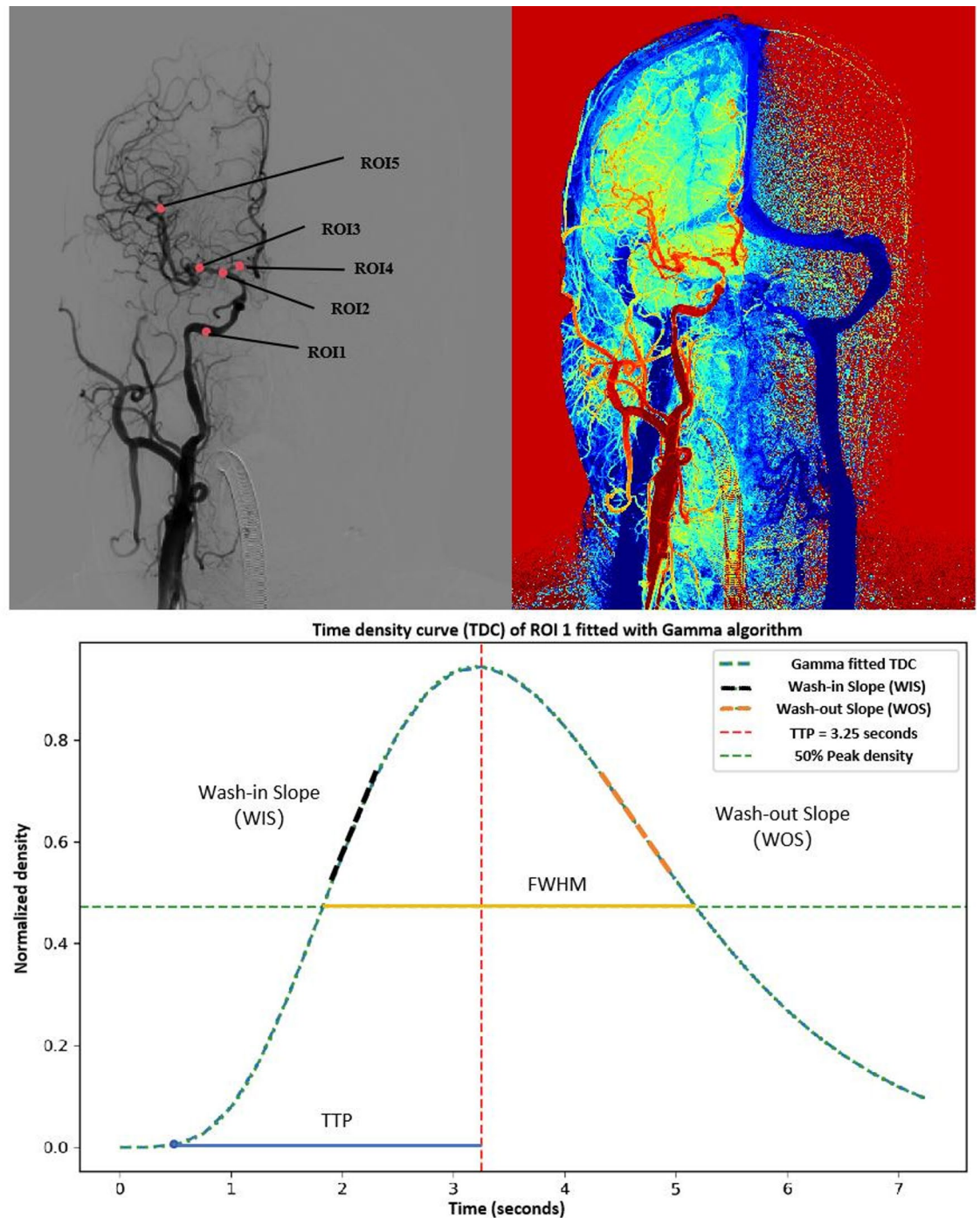


**Fig. 1.** The diagram illustrates the specific locations of the regions of interest (ROIs) and the method for extracting the time-density curve (TDC) and calculating relevant hemodynamic features. Upper, the exact positions of ROI1-5; Lower, the extraction of the TDC curve, followed by the use of Gamma fitting to construct a smoother TDC curve, and the calculation of corresponding hemodynamic parameters.

Fisher's exact test was used to assess differences, and the results were presented as the number of events along with their relative frequencies (%). A two-sided p-value of  $< 0.1$  was set as the threshold to indicate a statistically significant difference. Univariate analyses were conducted using SPSS (Version 25).

## Results

### Demographic characteristics

Between January 2024 and December 2024, a total of 381 patients diagnosed with acute ischemic stroke (AIS) and undergoing mechanical thrombectomy (MT) were screened. Ultimately, 171 patients with anterior circulation

occlusion who achieved successful recanalization and met the inclusion criteria were included in the study. The detail of the inclusion process was illustrated in the online Supplemental Fig. 1. Among the 171 AIS patients who achieved successful recanalization after MT, the median age was 66 years, and 117 patients (68.42%) were male. The median NIHSS score at admission was 16, and the median GCS score was 11. A total of 140 patients (81.87%) achieved an eTICI grade of 3, and 144 patients (84.21%) had good collateral circulation. The median number of thrombectomy attempts was 2, and the median puncture-to-reperfusion time was 42 min. Other perioperative characteristics, including the use of balloon angioplasty as an adjunctive treatment and stent implementation, are summarized in Table 1.

Patients were categorized as having hemorrhagic transformation (HT) if it was identified on post-procedure CT scans. The HT group was defined by the presence of hyperdense areas on postoperative CT compared to preoperative CT, including intracerebral hemorrhage, subarachnoid hemorrhage, or contrast extravasation, regardless of clinical symptoms. A total of 68 patients (68/171) were classified into the HT group. Symptomatic intracranial hemorrhage accounted for 18 cases (10.5%), while the remaining 50 cases (29.2%) were either asymptomatic intracranial hemorrhage or contrast extravasation. In the conventional univariate statistical analysis, compared with the non-HT group, patients with HT were older (median age 63 vs. 69,  $p=0.006$ ), required more attempts for thrombectomy (median 2 vs. 3,  $p=0.002$ ), and had a significantly higher NIHSS at presentation (median 15 vs. 18,  $p=0.077$ ). No significant differences between the two groups were observed in other characteristics, such as gender, occlusion site, puncture-to-reperfusion time, and final eTICI score. The detailed data are summarized in Table 1.

### QDSA characteristics and feature selection

Hemodynamic features were extracted from the gamma-variate-fitted time-density curve (TDC) for each patient. The ICC showed the TDC-derived features were all stable with the ICC > 0.75 (online Supplement Fig. 2), resulting in a total of 30 absolute value features and 9 relative value features (TTP ROI<sub>3-1</sub>, MTT ROI<sub>3-1</sub>, FWHM ROI<sub>3-1</sub>, TTP ROI<sub>4-1</sub>, MTT ROI<sub>4-1</sub>, FWHM ROI<sub>4-1</sub>, TTP ROI<sub>5-1</sub>, MTT ROI<sub>5-1</sub>, FWHM ROI<sub>5-1</sub>). Among the 39 hemodynamic features, the top 10 features with the highest coefficients selected by each feature selector were chosen for subsequent machine learning model construction. The features selected by the five feature selectors and their corresponding coefficients are listed in Table 2.

By summing the weights of each feature selected by all five selectors, the most frequently selected features with the cumulative weights > 1.5 were identified. The results showed that MTT and FWHM were the most frequently selected features influencing the final outcome, including relative MTT and relative FWHM of M3,

variables	All (n = 171)	HT (n = 68)	Non-HT (n = 103)	P value
age (y, median, IQR)	66 (19–86)	69 (33–85)	63 (19–86)	0.006*
Male, n(%)	117 (68.42)	44 (64.7)	73 (70.9)	0.396
Time since stroke onset (h, mean ± sd)	5.92 ± 5.13	6.10 ± 6.16	5.81 ± 4.33	0.853
Past Medical History (n, %)				
Hypertension	97 (56.72)	39 (57.35)	58 (56.31)	0.893
Diabetes mellitus	36 (21.05)	16 (23.53)	20 (19.42)	0.519
Atrial fibrillation	29 (16.96)	10 (14.71%)	19 (18.45%)	0.174
Admission NIHSS (median, IQR)	16 (6–40)	18 (6–40)	15 (6–35)	0.077*
Admission GCS (median, IQR)	11 (3–14)	10 (3–15)	11 (3–15)	0.393
Admission Aspect(mean ± sd)	7.42 ± 2.64	7.11 ± 2.64	7.63 ± 2.33	0.195
Occlusion site (n, %)				0.148
ICA	26 (15.20)	10 (14.71)	16 (15.53)	
MCA	98 (57.31)	34 (50.00)	64 (62.14)	
ACA	2 (1.18)	0 (0)	2 (1.94)	
ICA-MCA	44 (25.73)	23 (33.82)	21 (20.39)	
ICA-ACA	1 (0.58)	1 (1.47)	0 (0)	
Balloon assisted (n, %)	78 (45.61)	33 (48.53)	45(43.69)	0.534
Stent implementation (n, %)	43 (25.15)	17 (25.00)	26 (25.24)	0.971
Balloon expansion	78 (45.61)	33 (48.53)	45 (43.69)	0.534
Simple suctioning	13 (7.60)	5 (7.35)	8 (7.62)	0.948
PTR (min, median, IQR)	42 (3–78)	42 (13–78)	40.5 (3–72)	0.595
Attempts for Thrombectomy (median, IQR)	2 (1–6)	3 (1–6)	2 (1–5)	0.002*
ETICI				0.278
2b/2c	31 (18.13)	15 (22.06)	16 (15.53)	
3	140 (81.87)	53 (77.94)	87 (84.47)	

**Table 1.** Baseline characteristics of acute ischemic stroke patients treated with mechanical thrombectomy. HT: Hemorrhagic Transformation; ICA: Internal carotid artery; MCA: Middle cerebral artery; ACA: Anterior cerebral artery; PTR: Puncture-to-reperfusion time. \*  $p < 0.1$ .

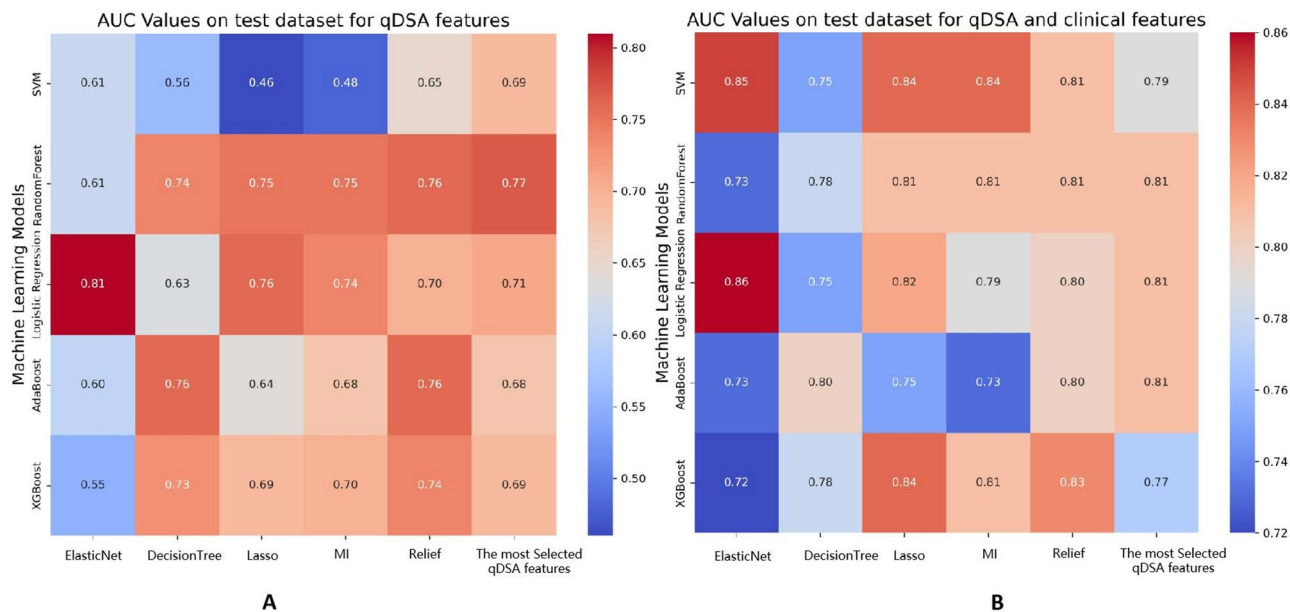


**Fig. 2.** The area under the curve (AUC) of machine learning models on the testing dataset. **(A)** The AUC of machine learning models on the testing dataset was constructed using selecting qDSA features filtered by different feature selection methods. **(B)** The AUC of machine learning models on the testing dataset was constructed using selected qDSA features combined with clinical features.

absolute FWHM of M3, absolute FWHM of C7, and relative MTT and relative TTP of A1. The cumulative weights were also listed in Table 2.

### Model performance evaluation

In Fig. 2A, a heatmap displays the AUC scores of the models constructed using qDSA features. The AUC scores ranged from 0.46 to 0.81, with a mean value of 0.68. Among the classifiers, the LogisticRegression classifier and the RandomForest classifier demonstrated superior performance, achieving a mean AUC value of 0.73 across different features. The best-performing model was the Elastic-LogisticRegression model, which achieved an AUC of 0.81 and an accuracy (ACC) of 0.74 on the test dataset (mean sensitivity 0.80, mean specificity 0.71, mean PPV 0.65, mean NPV 0.86, mean F1-score 0.71). A multivariate logistic regression model was constructed using clinical features including patient age, NIHSS at presentation, and the number of attempted thrombectomies, with an area under the ROC curve (AUC) of 0.68. When clinical features were incorporated into the model construction (Fig. 2B), the AUC scores ranged from 0.73 to 0.86, with a mean value of 0.79. This was significantly superior to the results of traditional clinical modeling. Compared to the models built solely with qDSA features, the LogisticRegression classifier again outperformed other classifiers, achieving a mean AUC value of 0.81 across its five models. The best-performing model in this scenario was still the Elastic-LogisticRegression model, which achieved an AUC of 0.86 and an ACC of 0.72 on the test dataset (mean sensitivity 0.88, mean specificity 0.62, mean PPV 0.60, mean NPV 0.92, mean F1-score 0.71).

The best performance of the qDSA alone model was constructed using qDSA features selected by the Elastic features selector and LogisticRegression algorithm. The ROC curves in different random states for the data split are presented in Fig. 3. The SHAP summary plot ranks features by their average absolute SHAP values, highlighting M1 MTT (Relative), M1 FWHM (Relative), and C7 FWHM as the most influential relative qDSA features (Fig. 3). The results highlight the critical role of FWHM and MTT in predicting hemorrhagic transformation (HT) following mechanical thrombectomy (MT). These hemodynamic parameters appear to be robust predictors of post-treatment bleeding events.

### Analysis of the selected hemodynamic features

During the multiple model constructions that followed multiple rounds of data splitting using different random seeds, hemodynamic features of the M1 segment revealed consistently elevated SHAP values for both relative MTT, relative FWHM, and absolute FWHM, indicating that this parameter exerted a substantial influence on the model. Building on these findings, we proceeded to analyze the relative hemodynamic characteristics of the M1 in detail. The relative MTT and FWHM of the M1 segment of the MCA were slightly higher in the HT group compared to the non-HT group, though there were no statistically significant differences between the two groups (FWHM: HT group: 1.00 vs. non-HT group: 0.75,  $p=0.44$ ; MTT: HT group: 0.72 vs. non-HT group: 0.65,  $p=0.83$ ). However, among the most selected features of qDSA, the relative MTT and FWHM of the M3 segment of the MCA were lower in the HT group compared to the non-HT group, with a statistically significant difference observed in FWHM (FWHM: HT group: 1.00 vs. non-HT group: 1.75,  $p=0.014$ ; MTT: HT group: 0.83 vs. non-HT group: 1.00,  $p=0.157$ , Fig. 4). This suggested that lower relative FWHM and MTT in the distal

Feature filters	Feature name	Coefficient	Weight	Calculate weight
Relief				
	M3 FWHM*	0.012	1	2
	M3 FWHM (Relative)*	0.009	0.9	3.3
	M3 MTT (Relative)*	0.008	0.8	2.6
	M3 MTT	0.007	0.7	1.2
	M1 FWHM	0.007	0.6	0.6
	A1 TTP	0.006	0.5	0.5
	C7 SI	0.006	0.4	0.7
	C7 FWHM*	0.006	0.3	2.5
	C7 MTT	0.005	0.2	0.2
	M3 SI	0.005	0.1	1.0
MutualInformation				
	M3 FWHM*	0.097	1	2
	M1 MTT	0.071	0.9	0.9
	M3 FWHM (Relative)*	0.069	0.8	3.3
	A1 FWHM	0.062	0.7	1.5
	A1 MTT (Relative)*	0.060	0.6	1.9
	M3 MTT	0.057	0.5	1.2
	A1 FWHM (Relative)	0.055	0.4	0.4
	C7 WOS	0.042	0.3	0.3
	C7 FWHM*	0.055	0.2	2.5
	A1 WOS	0.035	0.1	0.2
LassoRegression				
	A1 TTP (Relative)*	0.229	1	1.6
	M3 WIS	-0.202	0.9	0.9
	M3 MTT (Relative)*	0.177	0.8	2.6
	M3 FWHM (Relative)*	-0.159	0.7	3.3
	C7 FWHM*	-0.150	0.6	2.5
	A1 MTT (Relative)*	-0.123	0.5	1.9
	M1 MTT (Relative)	0.105	0.4	1.1
	M1 TTP	0.100	0.3	0.4
	C2-3 FWHM	0.091	0.2	0.2
	A1 FWHM	0.085	0.1	1.5
ElasticNet				
	C7 FWHM*	-0.191	1	2.5
	M3 FWHM (Relative)*	-0.144	0.9	3.3
	A1 SI	-0.136	0.8	0.8
	M1 MTT (Relative)	0.127	0.7	1.1
	A1 TTP (Relative)*	0.106	0.6	1.6
	M1 FWHM (Relative)	-0.103	0.5	0.5
	M3 TTP (Relative)	-0.100	0.4	0.4
	A1 MTT (Relative)*	-0.099	0.3	1.9
	M3 WOS	-0.092	0.2	0.2
	M1 TTP	0.084	0.1	0.4
DecisionTree				
Continued				

Feature filters	Feature name	Coefficient	Weight	Calculate weight
	M3 MTT (Relative)*	0.144	1.0	2.6
	M3 SI	0.119	0.9	1.0
	A1 MTT	0.084	0.8	0.8
	A1 FWHM	0.082	0.7	1.5
	A1 WIS	0.081	0.6	0.6
	A1 MTT (Relative)*	0.073	0.5	1.9
	C7 FWHM*	0.068	0.4	2.5
	C7 SI	0.066	0.3	0.7
	M1 SI	0.043	0.2	0.2
	A1 WOS	0.036	0.1	0.2

**Table 2.** The coefficient of hemodynamic features selected by different filters. # TTP: time to peak; MTT: mean transit time; WIS: wash-in slope; WOS: wash-out slope; FWHM: full width at half maximum; SI: stasis index. \* The most selected features with cumulative weights > 1.5.

area were associated with an increased ratio of hemorrhagic transformation. A narrower FWHM (lower value) usually implies a more concentrated and consistent blood flow velocity distribution in that region, and it also generally indicates faster blood flow. The simultaneous reduction of both FWHM and MTT (especially the statistically significant decrease in FWHM) strongly indicates that the blood flow velocity in the M3 perfusion territory is significantly faster in the HT group compared to the non-HT group, and the region is in a state of hyperperfusion.

## Discussion

The present study aimed to construct a predictive model for post-thrombectomy hemorrhagic transformation in patients with AIS by integrating quantitative digital subtraction angiography features with machine learning models. Traditional imaging prior to treatment like CT perfusion or MRI can confirm large-vessel occlusion and estimate core/penumbra, but it cannot assess whether recanalization will lead to hyperperfusion or incomplete microcirculatory reperfusion. Even with successful macro-vascular recanalization (eTICI 3), up to 30% of patients develop microcirculatory dysfunction. QDSA quantifies this by measuring parameters like FWHM and relative MTT, which reflect microvascular patency and flow homogeneity—information that pre-treatment imaging cannot capture. While CTP and MRI are non-invasive, post-MT CTP requires additional radiation and contrast administration (increasing kidney injury risk in elderly patients with comorbidities). MRI is often impractical post-MT due to logistical constraints (patient instability et al.). In contrast, qDSA uses the same intraprocedural DSA acquisition (standard for MT) and requires no extra contrast, radiation, or patient transfer—making it a “zero-cost” add-on to routine care. Our findings demonstrate that machine learning algorithms, particularly the Logistic Regression model, can effectively utilize clinical and hemodynamic features to predict HT, highlighting the potential of qDSA parameters in guiding personalized management strategies following MT. To the best of our team’s knowledge, this study is the first to employ machine learning models to predict HT using qDSA features.

Our study employed multiple machine learning algorithms to construct predictive models for HT. The Logistic Regression model demonstrated superior performance, achieving an average AUC of 0.81 when solely using qDSA features and an average AUC of 0.86 when combined with clinical features. This highlights the robustness and stability of the Logistic Regression algorithm in handling complex, multidimensional data. Machine learning algorithms link hemodynamic features to hemorrhagic transformation events, uncovering potential nonlinear relationships between the two groups. From the perspective of treatment, early detection of HT is important for at least three reasons. Firstly, early detection of intracranial hyperperfusion played a crucial role in postoperative blood pressure management. Current guidelines indicate that aggressive blood pressure reduction is not recommended after thrombectomy, with target systolic blood pressure > 140 mmHg or mean arterial pressure > 70 mmHg.<sup>14–16</sup> However, when signs of bleeding were detected, individualized blood pressure management was necessary to prevent further expansion of bleeding<sup>17</sup>. On the other hand, early identification of hemorrhagic transformation could alert clinicians to perform early follow-up cranial CT scans. If bleeding occurred, it could be managed promptly. Lastly, early recognition of bleeding was extremely important for the application of postoperative antiplatelet drugs. If a patient was identified as being at high risk for HT, the use of dual antiplatelet therapy and tirofiban after thrombectomy should be carefully considered. This is why our study did not distinguish between symptomatic intracranial hemorrhage and simple contrast extravasation when developing the predictive machine learning model (18 cases of sICH [10.5%] vs. 50 cases of asymptomatic intracranial hemorrhage or contrast extravasation [29.2%]). Even for asymptomatic contrast extravasation, early prediction or intervention is of great significance for preventing further increase in hemorrhage and avoiding cerebral vasospasm. This finding underscores the importance of qDSA-derived hemodynamic parameters in predicting HT, even independently of clinical characteristics. The model integrates seamlessly into routine MT workflow—qDSA images are acquired intra-operatively. Total turnaround time for prediction is 3–4 min (manual ROI placement + automated analysis), compatible with post-MT immediate management windows.

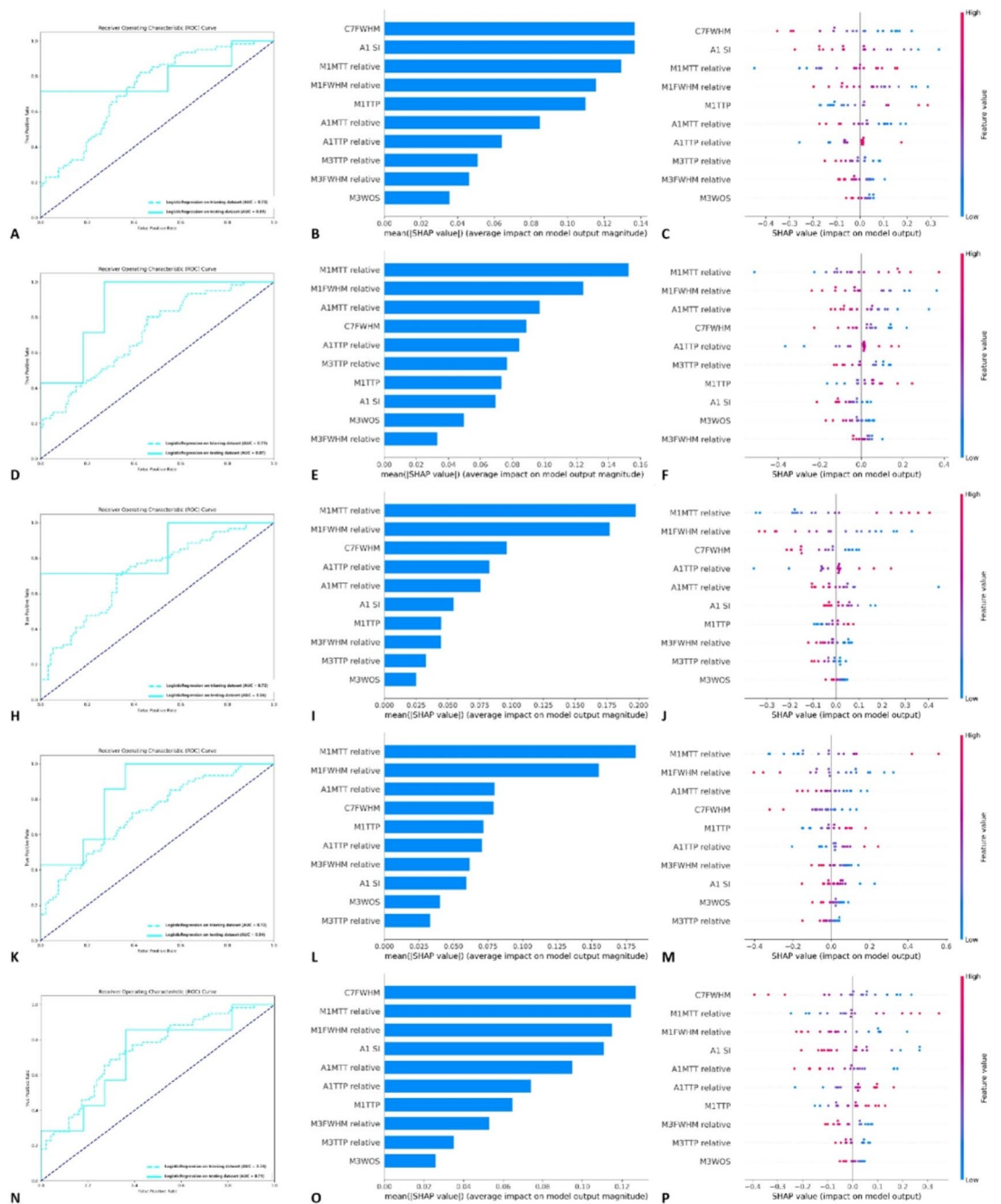


**Fig. 3.** (Left side) The ROC curve of LogistiRegression models constructed using the qDSA features selected by the Elastic algorithm and clinical features. (Middle and right side) The SHAP value of the 10 qDSA features was ranked, highlighting MTT and FWHM as the most influential qDSA features.

Hemodynamic parameters derived from qDSA, such as mean transit time (MTT) and full width at half maximum (FWHM), emerged as critical predictors of HT in our study. Specifically, the relative MTT and FWHM of the M3 segment of the middle cerebral artery (MCA) were lower in the HT group compared to the non-HT group (though the MTT showed no significant difference between groups). In a previous study focusing on MT, the authors proposed a U-shaped relationship between post-thrombectomy HT and MTT<sup>13</sup>. Specifically, both excessively high and excessively low MTT values were associated with an increased likelihood of HT. This finding suggests that the lack of a statistically significant difference in relative MTT values of the M3 segment between the two groups in our study may indicate a more complex, nonlinear relationship underlying this association. However, the aforementioned study had certain limitations in patient enrollment. The MTT values of the included patients were generally low, which contradicts the typical MTT values obtained from CTP, which are usually around 4. This discrepancy likely contributed to the limitations of exclusion bias.

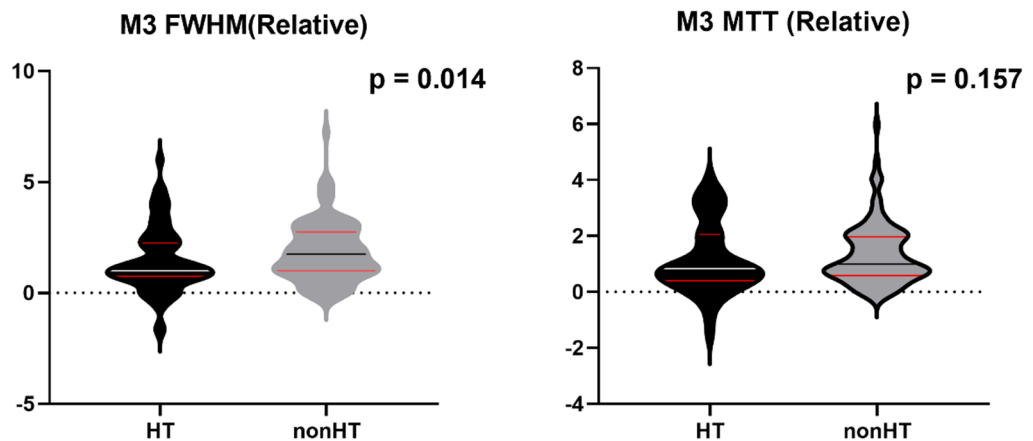


**Fig. 4.** The difference between the HT and non-HT groups on M3 FWHM (Relative) and M3 MTT (Relative). The relative FWHM of the M3 segment was significantly lower in the HT group compared to the non-HT group (HT group: 1.00 vs. non-HT group: 1.75,  $p = 0.014$ ). The relative MTT of the M3 segment was also lower in the HT group compared to the non-HT group; however, no significant statistical differences were observed (HT group: 0.83 vs. non-HT group: 1.00,  $p = 0.151$ ).

A lower MTT indicates that blood flows through the tissue in that region more quickly, which typically suggests an accelerated blood flow velocity in that area. In a previous study on cerebral arteriovenous malformations (AVMs), it was also confirmed that a shortened MTT was associated with Intralesional Microhemorrhages<sup>18</sup>. A narrower FWHM (lower value) usually implies a more concentrated and consistent distribution of blood flow velocity in that region, and it generally also indicates a faster blood flow velocity itself. A narrower FWHM and a shorter MTT indicate faster blood flow velocity and more concentrated blood flow distribution in the M3 perfusion territory, which may lead to hyperperfusion and subsequent HT. The accelerated blood flow and hyperperfusion observed in the distal vascular region (M3) are typical hemodynamic manifestations of reperfusion injury. In a recent study<sup>19</sup>, it was also mentioned that among the features predicting cerebral parenchymal hemorrhage after endovascular treatment, the blush sign in angiographic sequences, early venous filling, and TCD hyperperfusion state can accurately identify patients at high risk of hemorrhagic transformation. The current study offers an alternative quantitative approach. Hemodynamic features such as FWHM and MTT can reflect the state of hyperperfusion in brain tissue. When the FWHM and MTT values of distal vessels decrease postoperatively, vigilance for hemorrhagic events is warranted. Postoperative CT examinations should be conducted more proactively, with the interval shortened. Additionally, for such patients, whether to further pre-control postoperative blood pressure to baseline levels or even below the normal range is a key issue that requires focus in our subsequent studies. For these patients, attention should also be paid to the use of tirofiban and dual antiplatelet therapy (DAPT). It is necessary to administer these medications with more cautious dosing, while paying greater attention to the patients' drug sensitivity to DAPT. By integrating artificial intelligence methods, the study further explores the potential correlation between these features and the occurrence of bleeding.

There are also dissenting opinions. In another study focusing on TTP<sup>12</sup>, the authors included the hemodynamic parameters of the contralateral healthy side in their analysis. They found that TTP was significantly prolonged in symptomatic ICH, but there was no significant difference in TTP between ICH groups, including asymptomatic. The reason why qDSA data of the contralateral vessels are not included in our study is that the endpoint event of this research is postoperative hemorrhage, which has a relatively weak correlation with the hemodynamic status of the contralateral cerebral hemisphere. Another study also mentioned that prolonged cerebral circulation time (CCT) is a factor associated with HT<sup>11</sup>. However, both studies indicated that no significant differences were observed between the two groups in multivariate analysis.

In this study, we also found that patients who experienced hemorrhagic transformation after thrombectomy were significantly older and had a higher number of recanalization attempts compared to those who did not experience HT. These findings were consistent with previous studies. Prior research had also identified preoperative NIHSS score, preoperative ASPECTS score, collateral circulation, and recanalization attempts as important factors influencing post-thrombectomy bleeding<sup>20–22</sup>. However, traditional clinical scoring systems have lacked assessments of postoperative hyperperfusion. Therefore, the machine learning model developed in this study integrates traditional clinical evaluation indicators with indicators that reflect postoperative blood flow perfusion, constructing a more accurate predictive model. This approach provides a new method for future individualized assessment of patients' postoperative conditions and individualized perioperative management of thrombectomy patients.

Despite the promising results, our study has several limitations. Firstly, the retrospective design and single-center nature of the study may limit the generalizability of our findings. Future multi-center studies with larger sample sizes are needed to validate the predictive performance of our models. Secondly, Subgroup analysis was not further performed after including eTICI grades  $\geq 2b$ , which followed the inclusion criteria of the study by Zhiruo S et al.<sup>12</sup>. In our study, there were relatively few cases with eTICI grade 2b, while most were grade 2 C

or 3. Therefore, future studies may need to conduct subgroup analyses to develop machine learning models separately. Additionally, patients with large-area cerebral infarction and cerebral herniation were excluded from this study. In future research, we will expand the sample size and conduct a three-category study to further clarify the predictive role of hemodynamic parameters in different prognoses. Also, data expansion will not only improve the credibility of the model in this study but also eliminate the statistical bias caused by using a threshold of  $p < 0.1$  in univariate analysis. Lastly, external data validation is of great necessity.

## Conclusions

In conclusion, machine learning models integrating qDSA-derived hemodynamic features and clinical factors show promise for predicting post-MT HT, but their clinical utility should be interpreted in the context of existing evidence and requires validation in multi-center cohorts. Hemodynamic parameters such as M3 relative MTT and FWHM may serve as complementary tools for individualized risk stratification, alongside established clinical factors.

## Data availability

The datasets generated and analyzed in this study contain protected individual information. De-identified data can be provided by the corresponding authors upon reasonable request from editors or reviewers.

Received: 13 August 2025; Accepted: 19 January 2026

Published online: 22 January 2026

## References

1. Mead, G. et al. A systematic review and synthesis of global stroke guidelines on behalf of the world stroke organization. *Int. J. Stroke: Official J. Int. Stroke Soc.* **18**, 499–531 (2023).
2. William, J. P. et al. Guidelines for the early management of patients with acute ischemic stroke: 2019 update to the 2018 guidelines for the early management of acute ischemic stroke: A guideline for healthcare professionals from the American heart association/american stroke association. *Stroke* **50**, e334–e418 (2019).
3. Homan, T. et al. Unfavorable neurological long-term outcome despite etici 3 - what are the predictors? *Clin. Neurol. Neurosurg.* **245**, 108501 (2024).
4. Jean-Daniel, D. et al. Diabetes is an independent growth factor of ischemic stroke during reperfusion phase leading to poor clinical outcome. *J. Stroke Cerebrovasc. Dis.* **31**, 106477 (2022).
5. Blanca, T. et al. Delayed neurological improvement after full endovascular reperfusion in acute anterior circulation ischemic stroke. *Stroke* **52**, 2210–2217 (2021).
6. Noel vH, Helge, K. et al. Predictors of poor clinical outcome despite complete reperfusion in acute ischemic stroke patients. *J. Neurointerv. Surg.* **13**, 015889 (2020).
7. Shan-Shan, L. et al. Hyperperfusion on arterial spin labeling mri predicts the 90-day functional outcome after mechanical thrombectomy in ischemic stroke. *J. Magn. Reson. Imaging.* **53**, 1815–1822 (2020).
8. Yang, W. et al. Global hyperperfusion after successful endovascular thrombectomy is linked to worse outcome in acute ischemic stroke. *Sci. Rep.* **14**, 10024 (2024).
9. Mujanovic, A. et al. Perfusion abnormalities on 24-hour perfusion imaging in patients with complete endovascular reperfusion. *Stroke* **55**, 2315–2324 (2024).
10. Kangmo, H. et al. Angiography-based hemodynamic features predict recurrent ischemic events after angioplasty and stenting of intracranial vertebrobasilar atherosclerotic stenosis. *Eur. Radiol.* **34**, 2352–2363 (2023).
11. Yachen, J. et al. Effect of prolonged microcirculation time after thrombectomy on the outcome of acute stroke. *J. Neurointerv. Surg.* **15**, 1078–1083 (2022).
12. Zhiruo, S. et al. Combined collaterals and hemodynamic features to predict the prognosis in acute ischemic stroke patients undergoing mechanical thrombectomy. *J. Neurointerv. Surg.* **17**, e349–e355 (2024).
13. Jayme, C. K. et al. Exploring reperfusion following endovascular thrombectomy. *Stroke* **50**, 2389–2395 (2019).
14. Michael, D. G., Theodore, B., K Rose, D. & Alex Bou, C. Blood pressure management in ischemic stroke patients undergoing mechanical thrombectomy. *Neurol. Res. Pract.* **5**, 12 (2023).
15. Xiao, D. et al. Blood pressure management after endovascular thrombectomy: insights of recent randomized controlled trials. *CNS Neurosci. Ther.* **30**, e14907 (2024).
16. Pengfei, Y. et al. Intensive blood pressure control after endovascular thrombectomy for acute ischaemic stroke (enchanted2/mt): A multicentre, open-label, blinded-endpoint, randomised controlled trial. *Lancet* **400**, 1585–1596 (2022).
17. Wang, X. et al. Effects of blood pressure Lowering in relation to time in acute intracerebral haemorrhage: A pooled analysis of the four interact trials. *Lancet Neurol.* **24**, 571–579 (2025).
18. Xiaolin, C. et al. Higher flow is present in unruptured arteriovenous malformations with silent intralesional microhemorrhages. *Stroke* **48**, 2881–2884 (2017).
19. João André, S. et al. Aiming for Tici 4: angiographic and ultrasonographic predictors of parenchymal hemorrhage after successful thrombectomy. *J. Neurointerv. Surg.* 023273 (2025).
20. Aicheng, S. et al. Analysis of influencing factors of hemorrhagic transformation in patients with large vessel occlusion stroke after mechanical thrombectomy. *Am. J. Transl. Res.* **15**, 6304–6313 (2023).
21. Abdullah, R. et al. Risk of symptomatic intracranial hemorrhage after mechanical thrombectomy in randomized clinical trials: A systematic review and meta-analysis. *Brain Sci.* **15**, 63 (2025).
22. Xiang, Y., Jingjiang, P., Xiaoying, Z., Qiangqiang, H. & Bin, L. Predicting hemorrhagic transformation after thrombectomy in acute ischemic stroke: A multimodal score of the regional Pial collateral. *Neuroradiology* **64**, 493–502 (2021).

## Author contributions

H.L. and XY.M. designed this study and wrote the main manuscript text. P.C. and XY.G. finished the data acquisition and statistical analysis. The image post-processing was produced by YF.G. The conception and supervision of the study was done by CH.L.

## Funding

This work was supported by the research of the National Health Commission Capacity Building and Continuing Education Center (No. GWJJ2022100302).

## Declarations

### Competing interests

The authors declare no competing interests.

### Ethics statement

The studies involving humans were approved by the Ethics Committee of the First Hospital of Hebei Medical University. This study was performed in line with the principles of the Declaration of Helsinki.

### Additional information

**Supplementary Information** The online version contains supplementary material available at <https://doi.org/10.1038/s41598-026-37036-6>.

**Correspondence** and requests for materials should be addressed to X.M. or C.L.

**Reprints and permissions information** is available at [www.nature.com/reprints](http://www.nature.com/reprints).

**Publisher's note** Springer Nature remains neutral with regard to jurisdictional claims in published maps and institutional affiliations.

**Open Access** This article is licensed under a Creative Commons Attribution-NonCommercial-NoDerivatives 4.0 International License, which permits any non-commercial use, sharing, distribution and reproduction in any medium or format, as long as you give appropriate credit to the original author(s) and the source, provide a link to the Creative Commons licence, and indicate if you modified the licensed material. You do not have permission under this licence to share adapted material derived from this article or parts of it. The images or other third party material in this article are included in the article's Creative Commons licence, unless indicated otherwise in a credit line to the material. If material is not included in the article's Creative Commons licence and your intended use is not permitted by statutory regulation or exceeds the permitted use, you will need to obtain permission directly from the copyright holder. To view a copy of this licence, visit <http://creativecommons.org/licenses/by-nc-nd/4.0/>.

© The Author(s) 2026